

Measuring the role of surface chemistry in silicon microphotonics

Matthew Borselli,^{a)} Thomas J. Johnson, and Oskar Painter

Department of Applied Physics, California Institute of Technology,^{b)} Pasadena, California 91125

(Received 13 December 2005; accepted 7 March 2006; published online 31 March 2006)

Utilizing a high quality factor ($Q \sim 1.5 \times 10^6$) optical microresonator to provide sensitivity down to a fractional surface optical loss of $\alpha'_s \sim 10^{-7}$, we show that the optical loss within Si microphotonic components can be dramatically altered by Si surface preparation, with $\alpha'_s \sim 1 \times 10^{-5}$ measured for chemical oxide surfaces as compared to $\alpha'_s \leq 1 \times 10^{-6}$ for hydrogen-terminated Si surfaces. These results indicate that the optical properties of Si surfaces can be significantly and reversibly altered by standard microelectronic treatments, and that stable, high optical quality surface passivation layers will be critical in future Si micro- and nanophotonic systems. © 2006 American Institute of Physics. [DOI: 10.1063/1.2191475]

Because of the predicted saturation of “Moore’s law” scaling of transistor cost and density,¹ silicon-based microphotonics is being explored for the routing and generation of high-bandwidth signals.^{2–7} Historically, studies of Si surface and interface states have primarily focused on their electronic properties.^{8,9} Three exceptions to this are deep-level optical spectroscopy,¹⁰ cavity-ringdown spectroscopy,¹¹ and the ultrasensitive technique of photothermal deflection spectroscopy^{12,13} (PDS) which can measure fractional optical absorption down to $\alpha l \sim 10^{-8}$. None of the aforementioned techniques, however, is well suited for studying as-processed microphotonic elements. In this work we utilize a specially designed microdisk optical resonator to study the optical properties of surfaces typical in silicon-on-insulator (SOI) microphotonic elements in a noninvasive, rapid, and sensitive manner. Shown in Fig. 1, the high quality factor (Q) Si microdisk resonators used in this work provide surface-specific optical sensitivity due to the strong overlap of the top and bottom surfaces of the active Si layer with the electric field energy density of appropriately polarized bound optical modes of the microdisk.

A normalized measure of surface sensitivity for a guided-wave mode in a waveguide or resonator can be defined as $\Gamma'_s \equiv \Gamma_s/t_s$, where Γ_s is the fractional electric field energy overlap with a surface perturbation of physical depth t_s . If optical loss is dominated by interactions with the surface, then the modal loss coefficient per unit length (α_m) measured from experiment can be related to a fractional loss per pass through the surface given by $\alpha'_s = \alpha_m/\Gamma'_s$ [$= (2\pi n_g)/(\lambda_0 Q \Gamma')$], for a resonator with quality factor Q and modal group index of refraction n_g . As discussed in Ref. 14, for a true two-dimensional surface in which the perturbation depth is infinitesimal, α'_s is the most relevant quantity describing the surface and is equivalent to the fraction of power lost for a normal incident plane wave propagating across the surface. From finite-element method (FEM) simulations,¹⁵ shown in Fig. 1, the transverse magnetic (TM) polarization whispering gallery modes (WGMs) of the microdisk are $\sim 90\times$ more sensitive to the top and bottom $\langle 100 \rangle$ Si surfaces than the etched sidewall at the microdisk periphery; specifically, $\Gamma'_{\text{top}} = \Gamma'_{\text{bottom}} = 3.5 \times 10^{-3} \text{ nm}^{-1}$ and $\Gamma'_{\text{side}} = 8.1 \times 10^{-5} \text{ nm}^{-1}$. This implies that $\sim 0.2\%$ of the optical mode exists in a

single monolayer at the top (bottom) Si surface, while little of the mode sees imperfections at the microdisk perimeter. For the measured devices described below ($Q \sim 1.5 \times 10^6$), a surface absorption of one-tenth of the full linewidth was measurable, corresponding to a sensitivity limit of $\alpha'_s \sim 10^{-7}$.

The silicon microdisks in this work were fabricated from a SOI wafer from SOITEC, consisting of a 217 nm thick silicon device layer (p -type, 14–22 Ω cm resistivity, $\langle 100 \rangle$ orientation) with a 2 μm SiO₂ buried oxide (BOX) layer. Microdisks of 5 μm radius were fabricated,¹⁶ finishing with a 10 min acetone soak and piranha etch to remove organic materials. A 1 h dilute hydrofluoric acid (HF) solution comprised of five parts 18.3 M Ω de-ionized (DI) water to one part concentrated aqueous HF (49%) was used to remove a protective SiN_x cap and partially undercut the disk, as shown in the scanning electron microscope (SEM) micrograph in Fig. 1(a). The wafer was then rinsed in de-ionized water, dried with nitrogen (N₂), and immediately transferred into a N₂ purged testing enclosure.

The microdisk resonators were characterized using a swept-wavelength external-cavity laser (New Focus Velocity, $\lambda = 1420\text{--}1498$ nm, linewidth < 300 kHz) connected to a fiber taper waveguide probe.¹⁷ A fiber-based Mach-Zehnder interferometer was used to calibrate the high resolution, piezocontrolled wavelength scans to ± 0.01 pm linewidth accuracy. The micron-scale fiber taper probe was formed from a standard single-mode optical fiber and was used to evanescently excite the WGMs of the microdisk with controllable

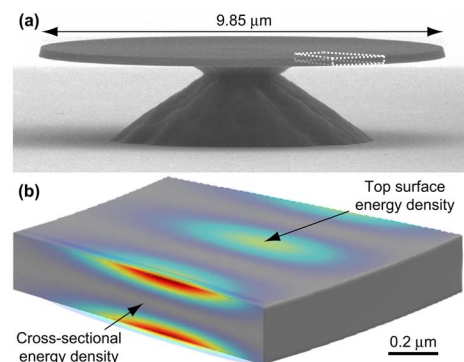


FIG. 1. (Color online) (a) SEM micrograph of a 5 μm radius SOI microdisk. (b) Zoomed-in representation of disk edge (white dashed box) showing a surface-sensitive TM polarized whispering gallery mode solved via FEM.

^{a)}Electronic mail: borselli@caltech.edu

^{b)}URL: <http://copilot.caltech.edu>

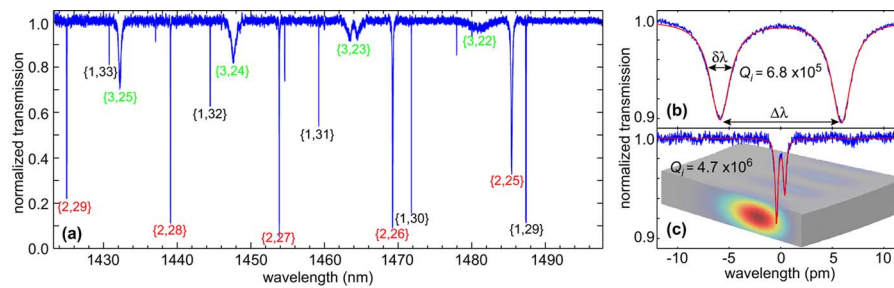


FIG. 2. (Color online) Normalized spectral transmission response of Si microdisk resonators. (a) Broad scan across $\lambda=1400$ nm band for a $5 \mu\text{m}$ radius microdisk with the fiber taper placed $0.6 \pm 0.1 \mu\text{m}$ away from the disk edge and optimized for TM coupling. The spectrum was normalized to the response of the fiber taper moved $3 \mu\text{m}$ laterally away from the disk edge. (b) High resolution scan of the $\text{TM}_{1,31}$ mode at $\lambda=1459$ nm in (a). $\Delta\lambda$ and $\delta\lambda$ indicate the CW/CCW mode splitting and individual mode linewidth, respectively. (c) Electric energy density plot and high resolution scan of a $40 \mu\text{m}$ radius microdisk, showing the reduced loss of a bulk TE WGM.

loading. Figure 2(a) shows the normalized spectral transmission response of a $5 \mu\text{m}$ radius microdisk resonator, illustrating clear families of modes having similar linewidth, $\delta\lambda$, and free spectral range (FSR). By comparison to FEM simulations of the Si microdisk, each mode in Fig. 2(a) was categorized and labeled as $\text{TM}_{p,m}$, where p and m are the radial and azimuthal numbers, respectively.

Owing to their large surface sensitivity (see Fig. 1), the spectral signature of the $\text{TM}_{1,m}$ modes was used to determine the quality of the optical surfaces. Figure 2(b) shows a high resolution scan across the $\text{TM}_{1,31}$ mode. The observed double resonance dip, termed a doublet, is a result of surface roughness coupling of the normally degenerate clockwise (CW) and counter-clockwise (CCW) propagating WGMs.^{16,18,19} The rate at which photons are backscattered is quantified by the doublet splitting, $\Delta\lambda$, while the rate at which photons are lost from the resonator is quantified by the intrinsic linewidth, $\delta\lambda$, of the individual doublet modes. From a fit to the transmission spectrum of Fig. 2(b), $\Delta\lambda=11.9$ pm and $\delta\lambda=2.2$ pm, corresponding to an intrinsic modal quality factor of $Q_i \equiv \lambda_0/\delta\lambda=6.8 \times 10^5$ for this $\text{TM}_{1,31}$ mode. This should be contrasted with the electric field energy density plot and transmission spectrum shown in Fig. 2(c) for a more confined, and less surface sensitive, TE WGM of a much larger $40 \mu\text{m}$ radius microdisk ($\Gamma'_{\text{top}}=\Gamma'_{\text{bot}}=1.2 \times 10^{-3} \text{ nm}^{-1}$ and $\Gamma'_{\text{side}}=2.3 \times 10^{-5} \text{ nm}^{-1}$). From the fit parameters ($\Delta\lambda=0.8$ pm, $\delta\lambda=0.3$ pm), the Q of the buried TE mode is $Q_i=4.7 \times 10^6$, corresponding to a loss per unit length of $\alpha_i=0.13$ dB/cm. This is nearly an order of magnitude smaller optical loss than that of the as-processed $\text{TM}_{1,m}$ modes, and provides an upper bound on the bulk Si optical loss of the SOI material.

The stark difference between the surface-sensitive TM and bulk TE modes indicates that the as-processed Si surfaces are far from optimal. Etch-induced surface damage on the microdisk sidewall can only account for a small fraction of this difference due to the enhanced sensitivity of the $\text{TM}_{1,m}$ to the top and bottom Si surfaces (comparison of the TM and TE modes in the same microdisk and with similar modal overlap with the microdisk edge bear this out). Damage to the top and bottom Si surfaces can stem from a variety of possible sources including chemical mechanical polishing, native oxide formation during storage, or adventitious organic matter.²⁰ In an attempt to repair the Si surfaces a series of chemical oxidation treatments were performed on the devices. The well-known process^{9,21,22} of repeated chemical oxidation in piranha ($\text{H}_2\text{SO}_4/\text{H}_2\text{O}_2$) and HF oxide stripping

was employed to controllably prepare the Si surfaces. Three cycles of the piranha/HF process, recipe shown in Table I, were applied to the as-processed devices. From the blueshift in the WGM resonances due to the three cycles of the piranha/HF process, an estimated 1.9 ± 0.1 nm of Si was removed from the surface of the microdisk. The fit to the $\text{TM}_{1,31}$ transmission spectrum, shown in Fig. 3(b), indicates that a significant improvement to the surfaces has also taken place, yielding a $\Delta\lambda=7.2$ pm and $\delta\lambda=1.1$ pm.

To separate the effects of the piranha oxidation and the HF etch, the sample was put through a piranha/HF/piranha treatment. The first cycle of piranha/HF was used to “refresh” the hydrogen passivation before reoxidizing the Si surface with piranha. Figure 3(c) shows the fit to the now barely resolvable $\text{TM}_{1,31}$ doublet yielding $\Delta\lambda=8.6$ pm and $\delta\lambda=5.6$ pm. The fivefold increase in linewidth and a negligible increase in doublet splitting is indicative of a significant activation of absorbing surface states without an increase in surface scattering. Removing the chemical oxide with the HF dip listed in Table I and retesting indicated that an oxide film equivalent to 2.8 ± 0.1 nm of SiO_2 had been present. The fit to the transmission spectrum of the $\text{TM}_{1,31}$ mode in Fig. 3(d) yielded fit parameters $\Delta\lambda=9.7$ pm and $\delta\lambda=1.2$ pm, showing that the optical damage to the Si surfaces caused by piranha oxidation was reversible.

As a final treatment to the $5 \mu\text{m}$ radii microdisks, we used the same $3 \times$ oxidation and stripping process as described in Table I, but with a HCl based chemistry (8:1:2 $\text{H}_2\text{O}:\text{HCl}:\text{H}_2\text{O}_2$, heated to 60°C) instead of the H_2SO_4 based chemistry. Figure 3(e) shows a graphical representation of the average behavior of all $\text{TM}_{1,m}$ modes in the 1420–1470 nm span after each chemical treatment. The results reveal that the HCl oxidation was slightly less effective at passivating the silicon surface than the piranha oxidation; however, it is expected that the optimum solution for chemical oxidation will depend upon the Si crystal orientation and previous chemical treatments.^{23,24}

TABLE I. Summary of piranha oxidation surface treatment.

Step	Composition ^a	Temp.	Time
Piranha	3:1 $\text{H}_2\text{SO}_4/\text{H}_2\text{O}_2$	100°C	10 min
$3 \times$ rinse	DI H_2O	23°C	30 s
HF dip	10:1 $\text{H}_2\text{O}/\text{HF}$	23°C	1 min
$2 \times$ rinse	DI H_2O	23°C	15 s

^aStandard concentration aqueous solutions.

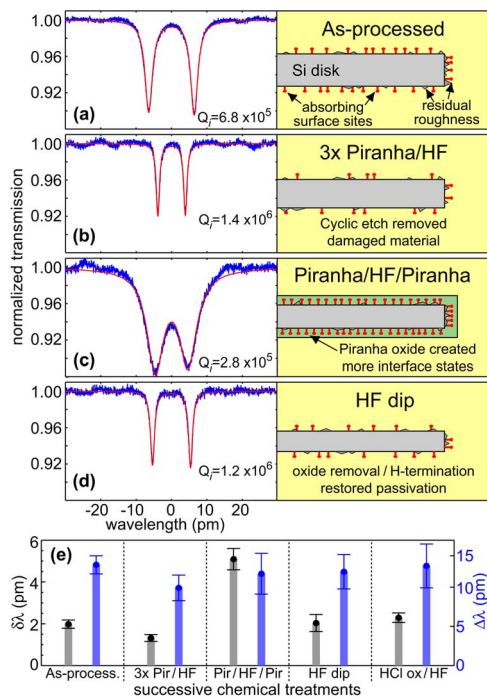


FIG. 3. (Color online) (a)–(d) Wavelength scan of the $TM_{1,31}$ doublet mode after each chemical treatment and accompanying schematic of chemical treatment. (a) As-processed, (b) triple piranha/HF cycle (Table I), (c) single piranha/HF/piranha step allowing measurement of piranha oxide, and (d) HF dip to remove chemical oxide from previous treatment and restore passivation. (e) Average intrinsic linewidth, $\delta\lambda$, and average doublet splitting, $\Delta\lambda$, for all $TM_{1,m}$ modes within the 1420–1470 nm spectrum after each chemical treatment step.

Although it has recently been observed²² that repeated chemical oxidation and removal of silicon can provide a smoothing action on etched sidewalls, the large shifts in optical loss with chemical treatment described above can be linked to surface-state absorption as opposed to surface scattering. Whereas the highly confined Si waveguide measurements to date have been sensitive to changes in loss as low as 1 dB/cm, the microdisks of this work are sensitive to changes of loss more than an order of magnitude smaller (<0.03 dB/cm) where surface chemistry is more likely to play a role. Indeed, as mentioned above the TM-polarized microdisk WGMs are selectively sensitive to the top and bottom Si surfaces which are extremely smooth in comparison with etched surfaces. The negligible change in average mode splitting, $\Delta\lambda$, with chemical treatment [Fig. 3(e)] is also indicative of little change in surface roughness. A complementary analysis²⁵ of power dependent transmission scans showed that $\sim 50\%$ of residual optical loss, after piranha/HF treatment and hydrogen surface passivation, is still due to surface-state absorption (bulk absorption is negligible at this level).

By comparing the cavity Q before and after the piranha oxide removal, a fractional surface absorption loss per pass of $\alpha'_{s,ox} \sim 1 \times 10^{-5}$ is estimated for the piranha oxide. This large fractional absorption in the $\lambda = 1400$ nm wavelength band ($\hbar\omega \sim 0.85$ eV) is attributed to single-photon absorption by midgap interface states. Such electronic interface states at the Si/(piranha)SiO_x interface have been observed in Ref. 26, with three sets of state-density maxima in the band gap of silicon occurring at 0.3, 0.5, and 0.7 eV referenced to the valence-band maximum, with a Fermi energy of

~ 0.4 eV. Thus, our observed surface absorption is most likely dominated by the transition from the filled 0.3 eV surface-state band to the conduction band at 1.1 eV. In comparison, the modal absorption loss of the hydrogen-passivated Si surface was measured²⁵ to be as small as $\alpha'_m \sim 0.08$ cm⁻¹, corresponding to a fractional surface absorption loss per pass of $\alpha'_{s,H} \sim 1 \times 10^{-6}$ for the top (bottom) Si active layer surface.

All of the measurements described above were performed in a N₂ purged environment over several weeks. Even in such an environment, however, changes in the hydrogen passivated surfaces were observed over times as short as a few days. Left in an unprotected air environment, degradation of the optical surface quality was evident in a matter of hours. Research and development of stable surface passivation techniques optimized for optical quality, akin to the gate oxides of CMOS microelectronics, will be a key ingredient in the future development of Si photonics. Our data suggest that surface chemistry as much as surface roughness will ultimately limit the performance of Si microphotonic devices, and further development of Si passivation techniques should be able to reduce optical losses by as much as an order of magnitude (towards the bulk *c*-Si limit) while improving the stability and manufacturability of future Si photonic components.

This work was supported by DARPA through the EPIC program. One of the authors (M.B.) thanks the Moore Foundation, NPSC, and HRL Laboratories.

¹D. A. Muller, Nat. Mater. **4**, 645 (2005).

²A. Liu, R. Jones, L. Liao, D. Samara-Rubio, D. Rubin, O. Cohen, R. Nicolaescu, and M. Paniccia, Nature (London) **427**, 615 (2004).

³Q. Xu, B. Schmidt, S. Pradhan, and M. Lipson, Nature (London) **435**, 325 (2005).

⁴O. Boyraz and B. Jalali, Opt. Express **12**, 5269 (2004).

⁵H. Rong, R. Jones, A. Liu, O. Cohen, D. Hak, A. Fang, and M. Paniccia, Nature (London) **433**, 725 (2005).

⁶T. Tanabe, M. Notomi, S. Mitsugi, A. Shinya, and E. Kuramochi, Opt. Lett. **30**, 2575 (2005).

⁷B. Song, S. Noda, T. Asano, and Y. Akahane, Nat. Mater. **4**, 207 (2005).

⁸D. V. Lang, J. Appl. Phys. **45**, 3023 (1974).

⁹J. Linnros, J. Appl. Phys. **84**, 284 (1998).

¹⁰A. Chantre, G. Vincent, and D. Bois, Phys. Rev. B **23**, 5335 (1981).

¹¹I. M. P. Aarts, B. Hoex, A. H. M. Smets, R. Engeln, W. M. M. Kessels, and M. C. M. van de Sanden, Appl. Phys. Lett. **84**, 3079 (2004).

¹²W. B. Jackson and N. M. Amer, Phys. Rev. B **25**, 5559 (1982).

¹³G. Amato and F. Fizzotti, Phys. Rev. B **45**, 14108 (1992).

¹⁴P. Blood, IEEE J. Quantum Electron. **36**, 354 (2000).

¹⁵S. M. Spillane, T. J. Kippenberg, K. J. Vahala, K. W. Goh, E. Wilcut, and H. J. Kimble, Phys. Rev. A **71**, 013817 (2005).

¹⁶M. Borselli, T. J. Johnson, and O. Painter, Opt. Express **13**, 1515 (2005).

¹⁷M. Borselli, K. Srinivasan, P. E. Barclay, and O. Painter, Appl. Phys. Lett. **85**, 3693 (2004).

¹⁸M. Gorodetsky, A. Pryamikov, and V. Ilchenko, J. Opt. Soc. Am. B **17**, 1051 (2000).

¹⁹B. E. Little, J.-P. Laine, and S. T. Chu, Opt. Lett. **22**, 4 (1997).

²⁰D. Fenner, D. Biegelsen, and R. Bringans, J. Appl. Phys. **66**, 419 (1989).

²¹Y. Chabal, G. Higashi, and K. Raghavachari, J. Vac. Sci. Technol. A **7**, 2104 (1989).

²²D. K. Sparacin, S. J. Spector, and L. C. Kimerling, J. Lightwave Technol. **23**, 2455 (2005).

²³S. Petitdidier, V. Bertagna, N. Rochat, D. Rouchon, P. Besson, R. Erre, and M. Chemla, Thin Solid Films **476**, 51 (2005).

²⁴H. Kobayashi, Y. Yamashita, Y. Nakato, T. Komeda, and Y. Nishioka, Appl. Phys. Lett. **69**, 2276 (1996).

²⁵M. Borselli, T. J. Johnson, and O. Painter (unpublished).

²⁶Y. Yamashita, K. Namba, Y. Nakato, Y. Nishioka, and H. Kobayashi, J. Appl. Phys. **79**, 7051 (1996).